This is a post-referee draft, the final version is available at

https://doi.org/10.1016/j.jeurceramsoc.2020.06.016

An investigation on burner rig testing of environmental barrier coatings for aerospace applications

Emine Bakan[a]*, Daniel E. Mack[a], Sandra Lobe[a], Dietmar Koch[b], Robert Vaßen[a]

[a] Forschungszentrum Jülich GmbH, Institute of Energy and Climate Research IEK-1, 52425 Jülich, Germany

[b] University of Augsburg, Institute of Materials Resource Management, 86159, Augsburg, Germany

*Corresponding Author. Forschungszentrum Jülich GmbH, Institute of Energy and Climate Research IEK-1, 52425 Jülich, Germany. Tel: +49 2461 61 2785; Fax: +49 2461 61 2455, e-mail: e.bakan@fz-juelich.de

In this study, burner rig testing of Si/$Yb_2Si_2O_7$ environmental barrier coating protected SiC-based ceramic matrix composites was conducted. Tests were performed at standard conditions as well as with liquid water injection to the flame. Furthermore, the influence of the impingement angle of the flame (45° vs. 90°) on water vapor corrosion was explored. Gas flow rates were adapted in each test to adjust 1250 °C at the sample surface. The comparison of test results showed that water injection advances the corrosion of the $Yb_2Si_2O_7$ topcoat and the impingement angle affects the size and shape of the corroded area on the sample surface.

Keywords: Environmental barrier coatings (EBC); very low-pressure plasma spray (VLPPS); SiC/SiC; Ytterbium silicates; burner rig test

1. Introduction

SiC/SiC Ceramic Matrix Composites (CMCs) can significantly improve the efficiency of gas turbine engines thanks to their high-temperature capability and low density [1]. In the engine atmosphere, however, oxidation of SiC and volatilization of the oxidation product SiO_2 take place as a result of the water vapor reaction at elevated temperatures [2]. At long times, simultaneous oxidation and volatilization reactions lead to a linear weight loss of SiC under such conditions [3]. To reach the desired service life of thousands of hours, therefore, the SiC/SiC components are shielded from the combustion gases using environmental barrier coatings (EBCs). A baseline EBC system consists of a bond coat and a volatilization barrier made of silicon and rare earth silicates (e.g. $Yb_2Si_2O_7$), respectively.

Degradation of EBC systems on SiC/SiC CMCs has been investigated under different test conditions in the literature. Steam thermal cycling tests with low gas velocity (e.g. few cm/s) but high water vapor partial pressure (e.g. 50-90% vol. H_2O at atmospheric pressure) revealed that the key degradation mechanism of EBCs is steam oxidation of the Si bond coat [4-6]. Water vapor permeates through the $Yb_2Si_2O_7$ topcoat, reacts with the bond coat and forms an amorphous SiO_2 scale at the interface. Above 1200 °C, the amorphous SiO_2 crystallizes into β-cristobalite, which transforms into α-cristobalite during cooling with a volume reduction of 3-7 %. This leads to cracking in the SiO_2 layer and eventually spallation of the EBCs. Laboratory experiments

conducted at higher steam velocity (e.g. 90-100 m/s) but with lower H_2O partial pressure (e.g. 10-20% vol. H_2O at atmospheric pressure) indicated that, as a result of the water vapor reaction of $Yb_2Si_2O_7$, volatile $Si(OH)_4$ forms according to the following reaction and leaves the more stable Yb_2SiO_5 phase behind [7, 8]:

$$Yb_2Si_2O_7 + 2H_2O = Yb_2SiO_5 + Si(OH)_4 \quad (1)$$

The remaining Yb_2SiO_5 layers were observed to be porous and micro cracked due to a ~26 % volume reduction in this transformation. The kinetics of the reaction was found to be highly microstructure dependent, i.e. thickness of the porous Yb_2SiO_5 was about 6 µm at the surface of a sintered $Yb_2Si_2O_7$ body, whereas it was about 15 µm at the surface of a heat-treated $Yb_2Si_2O_7$ coating under the same testing conditions (after 200 h testing at 1400 ℃) [8]. Porous Yb_2SiO_5 scale was also observed at the surface of the $Yb_2Si_2O_7$ coating under steam cycling conditions with low gas velocity [4]. But the thickness of the Yb_2SiO_5 was only about 12 µm after 2000 h testing at 1316 °C. Furthermore, Yb_2SiO_5 was vertically cracked possibly due to long term cyclic thermal loads.

2. Experimental procedure

In this study, burner rig test experiments of $Yb_2Si_2O_7$/Si coated SiC/SiC CMCs were conducted. $Yb_2Si_2O_7$ volatilization barriers (~225 µm) and Si bond coats (~100 µm) were deposited on SiC/SiC CMC disk shape substrates (~3300 µm, r=15 mm) (manufacturing details of the SiC/SiC material are available elsewhere [9]) using very low-pressure plasma spraying and high-velocity atmospheric plasma spraying processes, respectively. Details of the spray processes can be found in the earlier work [10]. In the standard burner rig testing (without water injection), at which thermal barrier coatings are evaluated, the samples sustain thermo-mechanical stresses during thermal cycling under through-thickness thermal gradients. This is achieved by heating the coated side of the sample to a determined surface temperature using a natural gas-oxygen burner, while the backside is cooled with compressed air to induce the temperature gradient. In the following cooling cycle after this high-temperature period, both sides of the sample are cooled down to room temperature by compressed air cooling. The temperature measurements of the coated surface and substrate backside were both measured by infrared pyrometry. The measurement of surface temperatures was performed using a long-wave infrared (LWIR) pyrometer as described in [11]. The temperature of the CMC substrate was measured through a better suited mid-wave infrared (MWIR) pyrometer which integrated to the cooling nozzle for direct access to the rear side. Emissivities were approximated as 1, accepting a slight underestimation of temperatures. Further details of the used test setup can be found elsewhere [12].

In the standard test conditions at which the first EBC sample was tested, the flame velocity calculated from the total flow rates of the gases (natural gas, oxygen, and air) and the cross-sectional area of the flame (the diameter is estimated as 20 mm) is about 8 m/s at the adiabatic flame temperature (about 2273 K) assuming the ideal gas behavior (Table 1). The burner flame contains about 49 vol. % H_2O as combustion product, assuming complete combustion of the natural gas with pure oxygen and ideal gas behavior. A second sample was tested by injecting liquid water into the burner flame. A peristaltic pump and water atomizer were used for the purpose and the water was axially injected into the flame with a flow rate of 120 g/h. As the evaporation of liquid water cools down the flame, the gas flow rates were adjusted to ensure the same surface temperature of the sample in both experiments (Table 1). The flame diameter was observed to reduce down to about 10 mm with the increased gas flow rates in the second experiment. Consequently, the flame velocity was estimated to increase up to 47 m/s under these conditions,

while the water vapor content in the flame was not significantly affected. Although a higher amount of water vapor was generated via combustion and additional water injection, the partial pressure of water vapor was estimated to remain similar as a result of additional air intake via the atomizer that increased the total gas flow rate. Finally, a third experiment was made to explore the effect of the impingement angle (IA) on the corrosion behavior. The IA was reduced from 90° (standard) to 45° and water injection was also used in this experiment. A summary of the test conditions is given in Table 2. The three-burner rig tests were conducted at a surface temperature (T_{surf}) of 1250 °C and a backside temperature of 650 °C. The calculated bond coat temperature using the thickness of the layers and thermal conductivity (λ) of the materials taken from the literature ($\lambda_{Yb2Si2O7}$=2.0 W/mK [13], λ_{Si}=30.0 W/mK [14], $\lambda_{SiC/SiC}$=9.8 W/mK (through-thickness) [15] at 1000 °C) was 1120 °C. The thicknesses of coatings, as well as the corroded layers which will be discussed below, were measured via image analyses. To perform this, a minimum of five images was taken from the edges and middle parts of the layers. Each sample was cycled 500 times with a high-temperature dwell time of 5 min and a cooling period of 2 min.

Table 1: Burner rig gas flow rates with and without water injection and estimated flame characteristics. (slph: standard liter per hour)

Condition	Total gas flow rate (slph)	Estimated flame velocity (m/s)	Estimated H_2O content in the flame (vol.%)
Standard	1146	8	49
With H_2O injection (120 g/h)	1611	47	53

Table 2: Burner rig test conditions.

	Test conditions				
Number of samples	Water injection	Impingement angle (IA)	Surface temperature	Backside temperature	Number of cycles
#1	No (standard)	90°	1250° C	650°C	500
#2	Yes	90°			
#3	Yes	45°			

3. Results and discussion

Fig. 1a-b shows the photo and cross-section images of the sample cycled under standard conditions (#1). It can be seen from the photo of the sample (Fig. 1a) that a color change was noticed in the central part of the sample after testing. Except for this change, no macroscopic damage was observed after 500 cycles. The cross-section scanning electron microscope (SEM, ULTRA 55, Carl Zeiss NTS GmbH, Oberkochen, Germany) image that was taken from the central part of the sample (Fig. 1b) also revealed no cracks in the microstructure. However, at the surface of the $Yb_2Si_2O_7$ layer (Fig. 1c), a thin layer of Yb_2SiO_5 was found. The composition of the Yb_2SiO_5 layer was confirmed by Raman Spectroscopy as will be further elaborated below. Higher porosity in the Yb_2SiO_5 compared to the $Yb_2Si_2O_7$ coating is a clear indication that it was transformed from $Yb_2Si_2O_7$ as a result of the water vapor reaction. At the Si interfaces after the test (Fig. 1d-e), no visible oxidation products were observed under the given magnifications.

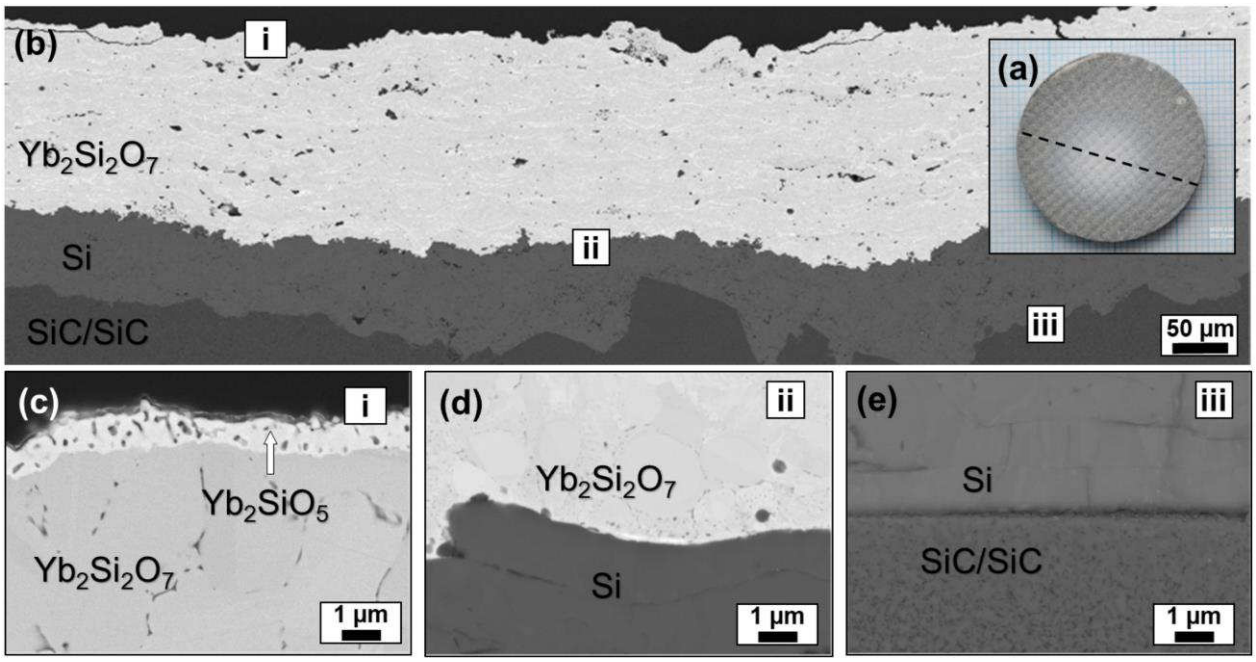

Figure 1: The photo of the 500 times cycled sample #1 at standard conditions (a). The cross-section SEM image of the same sample (b). The sample was sectioned through the dashed line shown in (a) and the image was taken approximately from the center of this line. High magnification SEM images of the topcoat surface (i) (c), topcoat bond-coat interface (ii) (d) and bond coat-substrate interface (iii) (e).

Fig. 2a-b shows the photos of the cycled samples #2 and #3, respectively. Similar to sample #1, the color change was also visible at the coated surfaces of these samples after the test. To find out whether this color change can be correlated with the presence of the Yb_2SiO_5 phase or not, the entire coated surface of the samples was measured by Raman Spectroscopy equipped with a 532 nm laser and automated focus tracking (Renishaw inVia^{TM} Qontor, Renishaw GmbH, Pliezhausen, Germany). Over 100000 spectra were collected from each sample with a step size of 100 µm (Fig. 2c-d). Exemplary spectra taken from Yb_2SiO_5 and $Yb_2Si_2O_7$ rich regions of the samples are shown in Fig. 2e. The extracted frequencies from the spectra of two phases coincide well with the results from the literature [16]. The intensity of the peaks, namely 925 cm^{-1} and 910 cm^{-1} of $Yb_2Si_2O_7$ and Yb_2SiO_5 phases, respectively, were used to calculate an intensity ratio (I_{P910}/I_{P925}) for every measurement point. The intensity ratios between 0.0-20.0 were then used to construct the spatially resolved phase maps shown in (Fig. 2c-d).

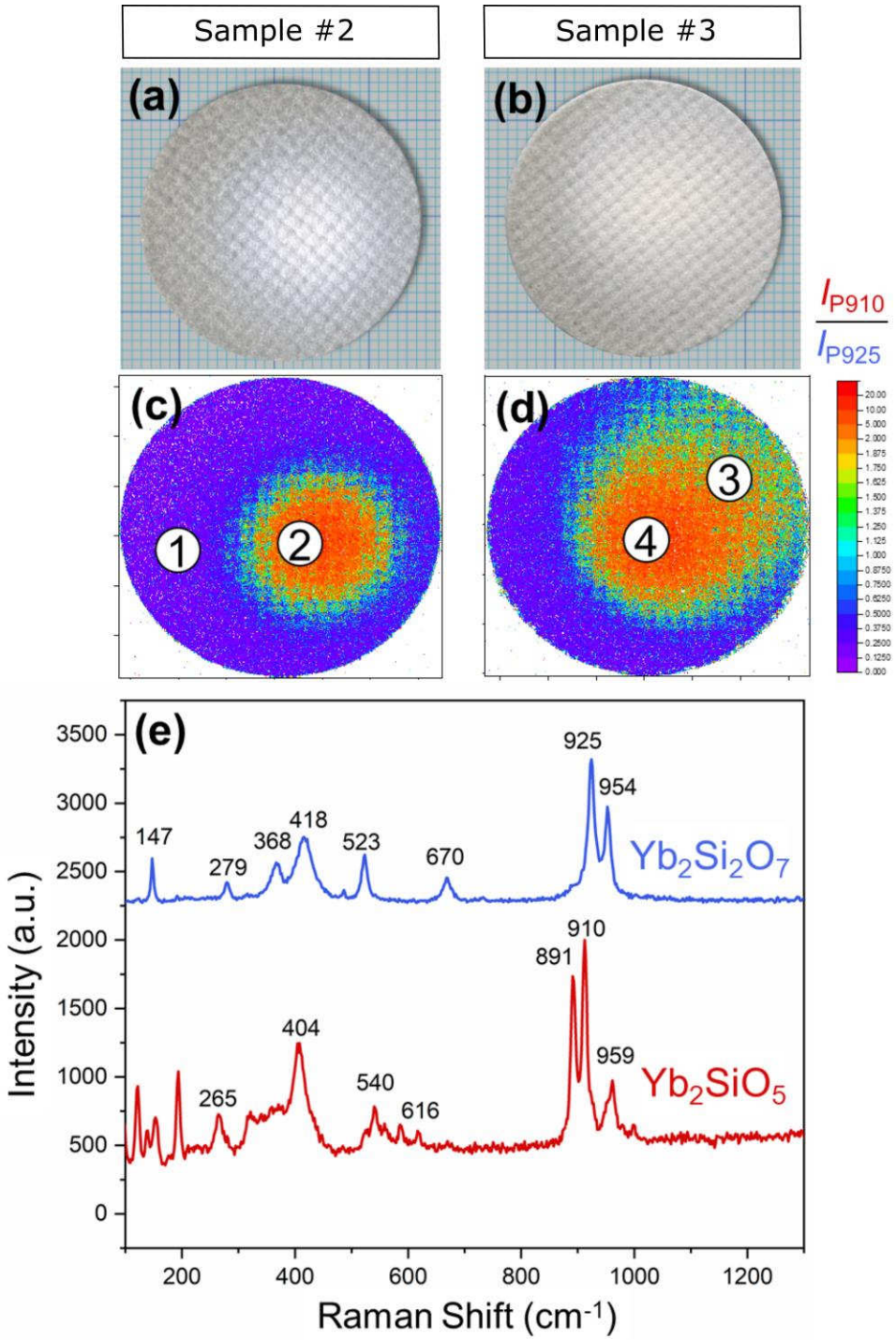

Figure 2: The photos of the 500 times cycled sample #2 (a), #3 (b). Spatially resolved Raman phase maps of sample #2 (c) and #3 (d) after the test. The color bar indicates the normalized intensity calculated from peak 910 (Yb_2SiO_5) and peak 925 ($Yb_2Si_2O_7$). Exemplary Raman spectra were taken from the $Yb_2Si_2O_7$ and Yb_2SiO_5 phase rich regions (e).

Cross-section SEM images taken from the marked regions 1-4 in Fig.2 c-d are shown in Fig. 3a-d. In region 1 on sample #2 (Fig. 3a), no continuous Yb_2SiO_5 layer was observed at the surface of $Yb_2Si_2O_7$. This result is in agreement with the Raman map because mainly the $Yb_2Si_2O_7$ phase

was detected in this region. In the region 2 of the same sample on the other hand, where Yb_2SiO_5 is the dominant phase according to Raman map, a porous Yb_2SiO_5 layer was found with an average thickness of 5.7 ± 1.8 µm (Fig. 3b). Similarly, in the regions 3-4 of sample #3, a porous Yb_2SiO_5 layer was identified at the surface of the $Yb_2Si_2O_7$ coating. The average Yb_2SiO_5 layer thicknesses were 5.8 ± 1.5 µm in region 3 and 7.3 ± 0.7 µm in the region 4. These results confirmed that the Yb_2SiO_5-rich red color regions in the Raman maps are indicating the corroded zones of the samples after the test. It should be also mentioned that similar to sample #1, no visible oxide scale was observed under SEM at the Si interfaces of sample #2-3.

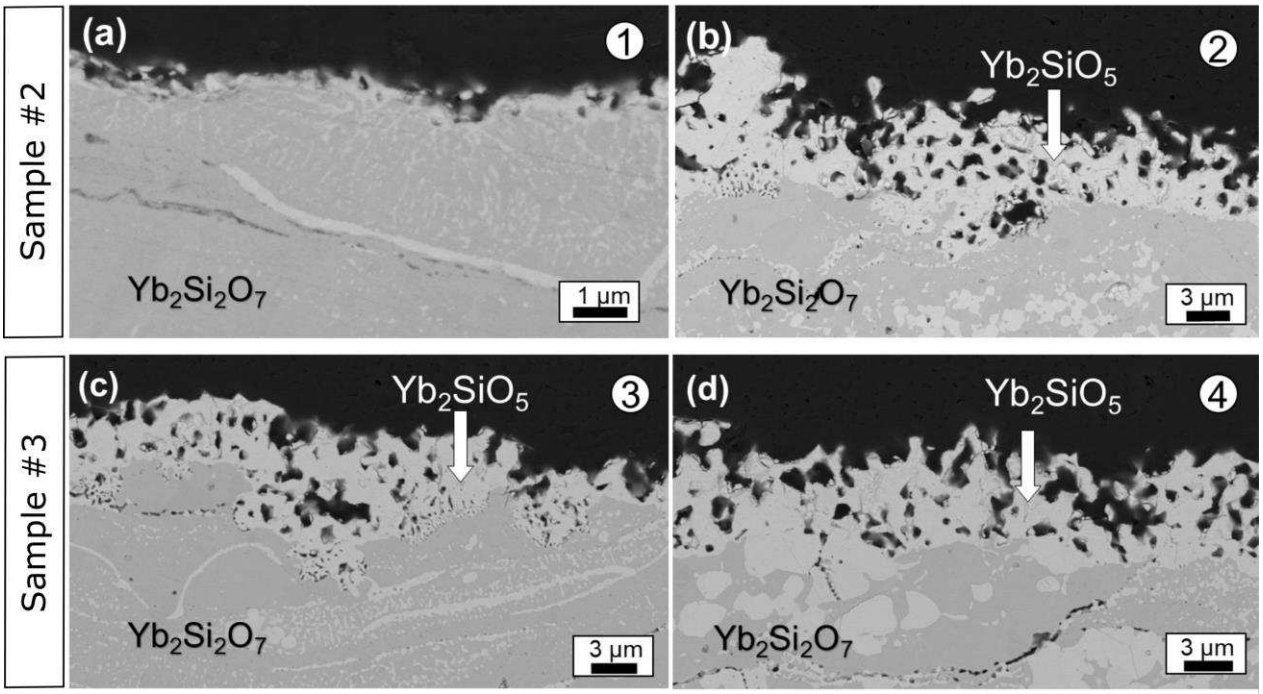

Figure 3: Cross-section SEM images of the thermally cycled samples #2-3 (a-d). The images are taken from the regions 1-4 shown in Fig. 2 c-d.

Based on these experimental results, the following conclusions can be drawn. In the standard test conditions, water vapor corrosion of the $Yb_2Si_2O_7$ already takes place, however, the corrosion can be promoted by water injection into the flame. This is evident from the increasing thickness of the transformed Yb_2SiO_5 layer which was ~0.8 µm in the standard conditions (#1) and reached up to ~6 µm by adding the water injection to the test procedure (#2). With the 120 g/h water injection, a small drop in the flame temperature is expected due to the volatilization enthalpy of the water. However, this was not critical for the test as the surface temperature of the sample could be kept at 1250°C with and without water injection. It appears that although the water vapor partial pressure ($P(H_2O)$ was also estimated to be similar in the experiments, the increased flame velocity (v) with the water injection leads to an increase in the volatility rate (k) according to the following relation:

$$k \propto exp\left(\frac{-\Delta H_r}{RT}\right) \times \frac{P(H_2O)^m \times v^n}{P_{total}^t} \quad (2)$$

where ΔH_r is the enthalpy of volatilization reaction, R is the universal gas constant, m is the number of moles of H_2O in the reaction (m=2), v is the gas velocity, n is the exponent of gas velocity ($n_{laminar}$

$_{flow}$=0.5, $n_{turbulent\ flow}$=0.8), P_{total} is the total pressure and t is the exponent of total pressure ($t_{laminar\ flow}$=0.5 and $t_{turbulent\ flow}$= 0.2). Assuming that the flow remained laminar regardless of the increased gas velocity, eq. (2) yields 2.4-fold higher k with the water injection. A turbulent flow under both conditions would lead to 4.1 times higher k with the higher gas velocity. In case that the flow was laminar in the standard conditions and turned to turbulent with water injection due to increased gas velocity, k is anticipated to be 7.6-times higher for the latter, which is in good agreement with the experimental findings of this study.

In all three experiments, Yb_2SiO_5-rich corroded regions were found to be concentrated in the central part of the samples. The thickest Yb_2SiO_5 layers suggest maximum temperature and/or gas velocity in these regions. Similar tests monitored by infrared imaging indicate temperature differences in the range of 50K to 200K from center of the heated area to the rim of specimen depending on injection of additives and inclination of the burner flame. At 45° IA, the corroded profile was evidently less symmetrical and larger (nearly 60% of the coated surface area) in comparison with that of 90°. This is possibly also related to differences in the temperature and flow velocity distributions at the sample surfaces when different IA are used. To understand that better, further investigations are required to establish the physics of the flow and the heat transfer from the impinging flame to the sample at different angles.

4. Conclusions

Burner rig tests of the EBC protected SiC/SiC CMCs substrates with and without water injection to the flame and at two different IA (45° and 90°) were conducted. The rest of the test conditions namely, surface and backside temperature and the number of cycles were kept constant. Results revealed that, although water vapor corrosion already takes place after 500 cycles (total ~42 h dwell time at high temperature) in the standard configuration (no water injection, at 90°), the corrosion affected area and thickness can be enlarged with the water injection at 45° IA. After this short time test at relatively low surface temperature (1250 °C), the thickness of the porous Yb_2SiO_5 layer was about 6 µm. This transformation rate (~0.14 µm/h) is significantly large when compared with the results in the literature (0.006 and 0.075 µm/h at [4, 8]), which indicates the capability of the adapted burner rig test. Considering the large coefficient of thermal expansion (CTE) mismatch between Yb_2SiO_5 and $Yb_2Si_2O_7$, and densification in the Yb_2SiO_5 at longer times due to sintering, Yb_2SiO_5 may spall off at a critical thickness. This would mean a reduction in overall coating thickness and an increase in the bond coat temperature which would accelerate the failure. Further experiments are therefore planned at higher surface temperatures aiming to increase the volatilization rates and bond coat temperatures.

Acknowledgments: The authors acknowledge the contributions of Ralf Laufs for plasma spray deposition of the samples, Martin Tandler for conducting burner rig tests, Christian Dellen for collecting the microscopy images, Hiltrud Moitroux for taking the photos of the samples and Bernd Mainzer for manufacturing the SiC/SiC plates.

References

[1] E. Bakan, D.E. Mack, G. Mauer, R. Vaßen, J. Lamon, N.P. Padture, in: O. Guillon (Ed.), Advanced Ceramics for Energy Conversion and Storage, Elsevier2020, pp. 3-62.
[2] N.S. Jacobson, J. Am. Ceram. Soc. 76(1) (1993) 3-28.
[3] E.J. Opila, J.L. Smialek, R.C. Robinson, D.S. Fox, N.S. Jacobson, J. Am. Ceram. Soc. 82(7) (1999) 1826-1834.
[4] B.T. Richards, K.A. Young, F. de Francqueville, S. Sehr, M.R. Begley, H.N.G. Wadley, Acta Mater. 106 (2016) 1-14.
[5] Y. Lu, L. Luo, J. Liu, C. Zhu, Y. Wang, J. Am. Ceram. Soc. 99(8) (2016) 2713-2719.

[6] K.N. Lee, J. Am. Ceram. Soc. 102(3) (2019) 1507-1521.
[7] E. Bakan, Y.J. Sohn, W. Kunz, H. Klemm, R. Vaßen, J. Eur. Ceram. Soc. 39(4) (2019) 1507-1513.
[8] E. Bakan, M. Kindelmann, W. Kunz, H. Klemm, R. Vaßen, Scripta Mater. 178 (2020) 468-471.
[9] B. Mainzer, R. Jemmali, M. Friess, D. Koch, in: D. Singh, M. Fukushima, Y. Kim, K. Shimamura, N. Imanaka, J. T. Ohji, A.a.M. Lanagan (Eds.), Proceedings of the 12th Pacific Rim Conference on Ceramic and Glass Technology2018, pp. 129-135.
[10] E. Bakan, D. Marcano, D. Zhou, Y.J. Sohn, G. Mauer, R. Vaßen, J. Therm. Spray Technol. 26(6) (2017) 1011-1024.
[11] F. Traeger, R. Vaßen, K.H. Rauwald, D. Stöver, Adv. Eng. Mater. 5(6) (2003) 429-432.
[12] T. Steinke, D. Sebold, D.E. Mack, R. Vaßen, D. Stöver, Surf. Coat. Technol. 205(7) (2010) 2287-2295.
[13] Z. Tian, L. Zheng, Z. Li, J. Li, J. Wang, J. Eur. Ceram. Soc. 36(11) (2016) 2813-2823.
[14] P.D. Maycock, Solid-State Electronics 10(3) (1967) 161-168.
[15] X. Dong, Y.C. Shin, J. Nucl. Mater. 512 (2018) 268-275.
[16] T. Ogawa, N. Otani, T. Yokoi, C.A.J. Fisher, A. Kuwabara, H. Moriwake, M. Yoshiya, S. Kitaoka, M. Takata, PCCP 20(24) (2018) 16518-16527.